

## Large omnidirectional band gaps in metallodielectric photonic crystals

Shanhui Fan, Pierre R. Villeneuve, and J. D. Joannopoulos

*Department of Physics, Massachusetts Institute of Technology, Cambridge, Massachusetts 02139*

(Received 25 March 1996; revised manuscript received 14 June 1996)

Using a finite-difference time-domain method, we study the band-structure and transmission properties of three-dimensional metallodielectric photonic crystals. The metallodielectric crystals are modeled as perfect electrical conducting objects embedded in dielectric media. We investigate two different lattice geometries: the face-centered-cubic (fcc) lattice and the diamond lattice. Partial gaps are predicted in the fcc lattice, in excellent agreement with recent experiments. Complete gaps are found in a diamond lattice of isolated metal spheres. The gaps appear between the second and third bands and their sizes can be larger than 60% when the radius of the spheres exceeds 21% of the cubic unit cell size. A possible fabrication scheme for this structure is proposed and transmission calculations are performed. [S0163-1829(96)02040-1]

### I. INTRODUCTION

Recently there has been a drive by experimental groups to incorporate metals into all-dielectric photonic crystals.<sup>1-3</sup> In particular, Brown and McMahon have recently demonstrated the existence of a large photonic band gap along the (111) direction of a face-centered-cubic (fcc) structure composed of metal spheres embedded in dielectric media.<sup>2</sup> As transmission experiments were performed along only one direction, the possible omnidirectional nature of this gap was not determined. Theoretical support would be very useful in the determination of the completeness of the photonic gap and ultimately in the design and optimization of metallodielectric photonic crystals with large omnidirectional gaps.

Metals, however, offer new challenges for the theoretical investigation of photonic band-gap materials. Among several approaches in recent years,<sup>4-8</sup> three-dimensional calculations<sup>4,5,8</sup> concentrate only on structures with spatial periods comparable to the plasma wavelength, which usually lies in the ultraviolet region. In this particular frequency range, dispersion and absorption effects must be taken into account in order to obtain the correct electromagnetic response. However, instead of working in the range of the plasma frequency, we have chosen to investigate the existence of photonic band gaps in metallodielectric structures in the microwave region, which is several orders of magnitude lower than the plasma frequency. Our choice was motivated by recent experiments in the microwave region<sup>1-3</sup> where metals are essentially lossless and can be accurately modeled as perfectly electrical conductors.

In this paper, we apply simple schemes based on finite-difference time-domain (FDTD) methods to calculate both the photonic bands and the associated field distribution of perfect crystals. The FDTD methods are also used to obtain transmission spectra through finite-thickness samples in order to make direct comparisons with experiments. After a brief description of the computational methods in Sec. II, we will present results for a variety of fcc and diamond crystals in Sec. III.

### II. COMPUTATIONAL METHOD

Finite-difference time-domain methods are widely used in analyzing interactions between electromagnetic waves and

complex structures containing dielectric and/or metallic objects.<sup>9</sup> The general procedure involves approximating Maxwell's equations in real space using finite differences, imposing appropriate boundary conditions, and explicitly time marching the fields to obtain the direct time-domain response, from which a wide variety of information can be extracted.

For simplicity, we use Yee's discretization scheme to solve Maxwell's curl equations.<sup>10</sup> All field variables are defined on a rectangular grid. Electric and magnetic fields are temporally separated by one-half time step. In addition, they are spatially interlaced by half a grid cell. Based on this scheme, center differences in both space and time are applied to approximate Maxwell's equations. Since all grid cells are rectangular in shape, arbitrary geometries are approximated by staircases. The validity and limitations of staircase approximations are discussed in Ref. 11.

Inside the metallic objects, all electric-field components are set to zero at each time step, since every electric-field component vanishes in a perfect conductor. With the metallodielectric interface placed at the integer grid plan in Yee's lattice, the tangential components of the electric field and the normal component of the magnetic field vanish at the interface. The correct boundary condition is therefore ensured.

In order to compute the field at any given grid point, we must know the value of the field at every adjacent point on the grid. With a finite computational cell, information from nodes outside the cell is not available. Fields at the nodes on the boundaries therefore have to be updated using boundary conditions. Depending on the purpose of the simulation, either absorbing or periodic boundary conditions are applied. This and other aspects of the computational methods specific to either transmission or band-structure calculations are discussed below.

#### A. Transmission calculations

While the methods described above can be applied to study propagation of electromagnetic waves in arbitrary structures, we are primarily concerned here with transmission of normally incident plane waves through a slab of photonic crystal, since the transmission can be directly measured

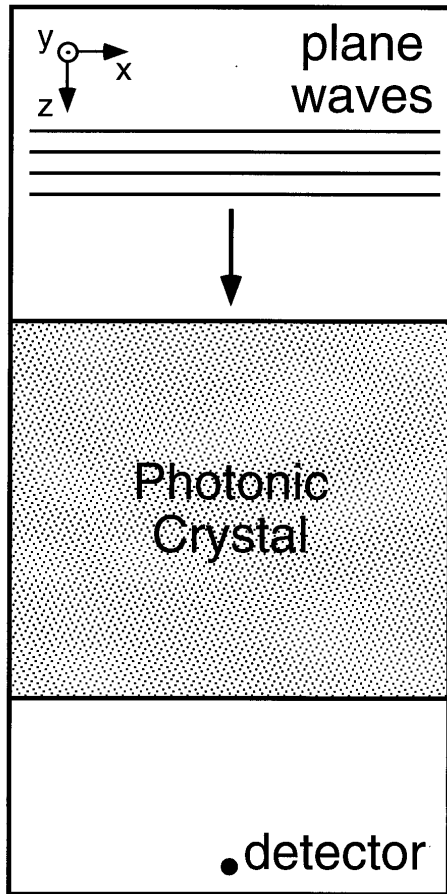


FIG. 1. Schematic of the computational cell used in the transmission calculation.

by experiments.<sup>2</sup> A schematic of the computational cell is shown in Fig. 1. A slab of photonic crystal is placed in the middle of the cell with its top and bottom surfaces normal to the  $z$  direction. Plane waves propagating along the  $z$  axis are generated by exciting a plane of identical dipoles in phase. On the other side of the crystal, the field amplitude, is monitored at a single point, marked “detector” in Fig. 1.

Mur’s second-order absorbing boundary conditions<sup>12</sup> are used at the top and bottom edges of the computational cell. Plane waves hitting these boundaries get absorbed. On all other boundaries, we use periodic boundary conditions. By placing one unit cell of a slab of photonic crystal in the computational cell, we can simulate plane waves normally incident upon a slab with *infinite* extent in the  $x$  and  $y$  directions.

Instead of studying the steady-state response, one frequency at a time, we choose to send a single pulse of light with a wide frequency profile. The incident amplitude is calibrated at the detector point by running a simulation without the crystal. Simulations are then performed with the crystal present, the amplitude at the detector describing the transmitted wave. The transmitted and incident amplitudes are then transformed into the frequency domain using fast Fourier transformations. The transmission coefficients are determined by taking the square of the ratio between the two amplitudes.

## B. Band-structure calculations

Time domain simulations can also be used to obtain band-structure information. The computational domain is chosen to be a unit cell of the infinite crystal. Fields at nodes outside the domain are related to fields inside by Bloch’s condition

$$\mathbf{E}(\mathbf{r} + \mathbf{a}, t) = e^{i\mathbf{k} \cdot \mathbf{a}} \mathbf{E}(\mathbf{r}, t), \quad (1)$$

where  $\mathbf{r}$  is the position vector of a node in the domain,  $\mathbf{a}$  is a lattice vector, and  $\mathbf{k}$  is the wave vector. After the initial excitation, fields oscillate in a steady state that is a linear combination of several eigenstates with the same wave vector  $\mathbf{k}$ . Frequencies of these eigenstates can be obtained by a Fourier transformation of the time-domain amplitude at a given point. The resulting spectrum is composed of a discrete set of peaks, where each peak corresponds to an eigenfrequency. Similar methods have been used in determining phonon dispersion in semiconductors<sup>13</sup> and in calculating various electromagnetic wave properties in ordered and disordered dielectric structures.<sup>14</sup>

Modes in the computational cell are excited using one or several point dipole sources with Gaussian frequency-profile amplitudes. The oscillation period and the width of the Gaussian are chosen such that the excitation spectrum covers the frequency range of interest. In determining the band structure, we use a short pulse in time that excites a wide frequency range. Both the dipoles and the point where the field is recorded are placed away from all the symmetry planes, so that modes with different symmetries can be excited and recorded in one simulation. Instead of exciting several modes simultaneously using a pulse with a wide spectral range, we can also use a narrow source (i.e., long duration in time) to selectively excite only one eigenstate at a specific frequency. The symmetry of the steady state can further be specified by placing the dipoles in appropriate symmetrical configurations.

As discretization is performed on a rectangular lattice, a natural choice for the computational domain is rectangular. For fcc lattices, a cubic unit cell is employed, which contains four fcc primitive cells. As Eq. (1) only determines the phase relations between different *cubic* cells, the band structure obtained is a *folded* version for the underlying fcc lattice. To obtain *unfolded* band structures we need to specify the phase relation across different *primitive* cells. This is achieved by placing a dipole in each of the four primitive cells. The dipoles are separated by a fcc lattice vector, the relative phase between them satisfying Bloch’s theorem.

We study convergence of the methods by comparing the size of the gap for a given structure with different density of grid points. A detailed convergence study and specific examples of the above methods are presented below.

## III. RESULTS AND DISCUSSIONS

### A. fcc structures

We study a fcc structure proposed by Brown and McMahon.<sup>2</sup> The structure is constructed by stacking several layers of Teflon ( $\epsilon=2.1$ ), each layer containing a triangular lattice of cylindrical air holes with a metal sphere inserted in each hole. The layers are stacked along the (111) direction in a staggered fashion with an *ABC* repeating unit. The thick-

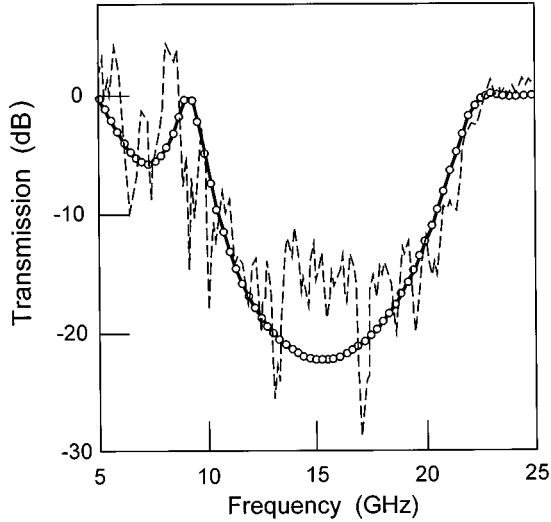


FIG. 2. Transmission spectra through a slab of a fcc metallodielectric photonic crystal. The solid line is obtained from theoretical calculation; open circles are data points. The broken line corresponds to experimental results, as described in Ref. 2.

ness of the slab and the lattice constant of the triangular arrays are chosen to form a fcc lattice. A detailed description of the structure is found in Ref. 2.

Using the method described in Sec. II A, we calculate transmission coefficients of normally incident plane waves through a crystal that contains one  $ABC$  repeating unit, in conformity with the experiments. In Fig. 2 the results are compared to experimental data, which were obtained using a cubic unit cell size of 0.43 in. Our simulations show the existence of a large gap extending from 9 to 23 GHz, with a maximum rejection of 22 dB, and the occurrence of a smaller gap between 5 and 9 GHz, all in excellent agreement with experiment. The rapid oscillations in the experimental spectrum are due to noise in the measurement.

We compute the band structure for the crystal using the method described in Sec. II B. A  $32 \times 32 \times 32$  cell is used for the calculation. We obtain the band-structure plot by analyzing the spectrum for each  $k$  point. The spectra at  $\Gamma$ ,  $L$ , and  $X$  are shown in Fig. 3(a) as examples. The band structure is plotted in Fig. 3(b), with the wave vector at the  $L$  point parallel to the axis of the air cylinders. A large gap exists along this direction between the frequencies  $f=0.42c/a$  and  $0.77c/a$ . In the specific case where the lattice constant  $a$  is equal to 0.43 in., the gap occurs between 11.5 and 21.2 GHz, in agreement again with the transmission experiments. The small discrepancy between the frequencies at the edges of the gap arises from the finite size of the experimental sample. The maxima in the transmission spectrum at the edges of the gap do not correspond exactly with the position of the band edges for the infinite crystal. The smaller gap at lower frequency finds no corresponding gap in the band structure in the infinite crystal. It is probably due to a Fabry-Perot oscillation in the finite-size sample. Figure 3(b) clearly shows that there is no omnidirectional gap for this crystal. The gap along the  $L$  direction does not extend to the directions of  $U$  and  $W$ .

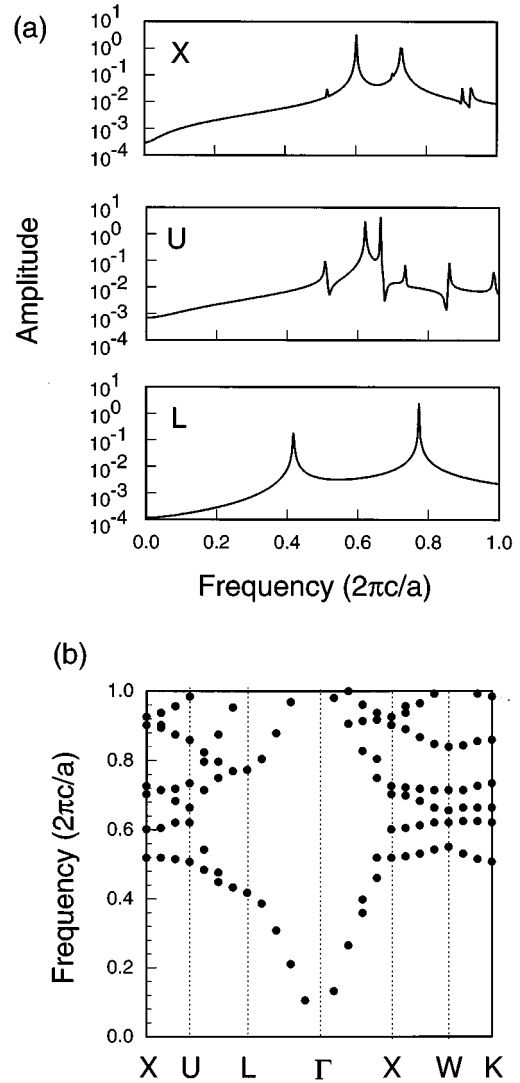


FIG. 3. (a) Spectral amplitude at several  $k$  points for the fcc metallodielectric photonic crystal. (b) Bands for the same fcc structure. Each dot corresponds to a peak in the spectral amplitude at a specific  $k$  point.

## B. Diamond structure

To search for a metallodielectric photonic crystal with an omnidirectional gap we consider a diamond lattice of metal spheres. The diamond lattice is a natural choice since large photonic band gaps have been predicted in all-dielectric crystals with a diamond structure.<sup>15</sup> A schematic of a diamond lattice is shown in Fig. 4. The radius of the spheres can be varied to tune the photonic bands. The spheres do not overlap with each other if the radius is smaller than  $0.2165a$ , where  $a$  is the size of the cubic unit cell. We focus our attention on nonoverlapping spheres, as unconnected spheres prevent long-range conduction currents. Such currents would contribute to undesirable Ohmic losses that increase rapidly with frequencies.

### 1. Band structure

The band structure is shown in Fig. 5 for the specific case where the radius is equal to  $0.21a$ . The spheres are embed-

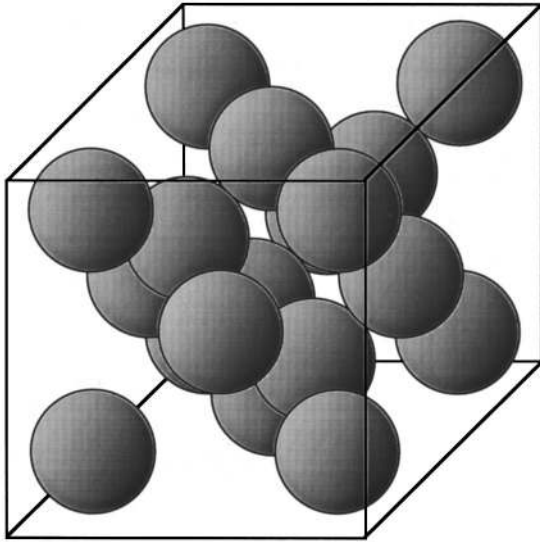


FIG. 4. Schematic of a diamond structure with nonoverlapping metallic sphere on each lattice site.

ded in Teflon ( $\epsilon=2.1$ ). The bands are calculated using a  $64 \times 64 \times 64$  grid. We find that there exists a full photonic band gap in which electromagnetic waves are forbidden to propagate in any direction. The lower edge of the gap is located at the  $W$  point of the second band and the upper edge is located at the  $X$  point of the third band. The gap covers the frequency range between  $0.43c/a$  and  $0.68c/a$ . The lower band is almost entirely flat along the  $X-U$  and the  $W-X$  lines on the surface of the first Brillouin zone. The size of the gap, defined as the gap width to midgap frequency ratio ( $\delta\omega/\omega_g$ ), exceeds 45%, which is significantly larger than the biggest gap ever reported in conventional all-dielectric photonic crystals.

## 2. Nature of the gap

In the metallodielectric systems studied above, the metallic spheres form impenetrable cores for electromagnetic waves. The field amplitudes for both the upper and the lower bands therefore are entirely distributed in the *uniform* dielectric. This behavior is in sharp contrast to conventional all-dielectric photonic crystals. In conventional crystals, the gap originates from the difference in field distribution between a low-frequency “dielectric” band, which has most of its displacement field concentrated in the high-dielectric region, and a high-frequency “air” band, which has its field penetrating more into the low-dielectric region.<sup>16</sup>

To probe into the origin of the gap in metallodielectric systems we choose to study the field distributions of the normal modes at the  $X$  point in the lower and upper bands. Each eigenmode is selectively excited by using sources with a narrow spectral width, performed by oscillating the dipole sources at a given frequency for a long duration. The spectra of the resulting steady states are shown in Fig. 6(a). Each spectrum contains only one peak, indicating the presence of a single eigenstate. The cross section of the power density in the magnetic fields is shown along the  $(110)$  plane in Fig. 6(b) for both the lower and the upper bands. We see that, in the lower band, the field is extended throughout the open region in the lattice, while in the upper band, the field is

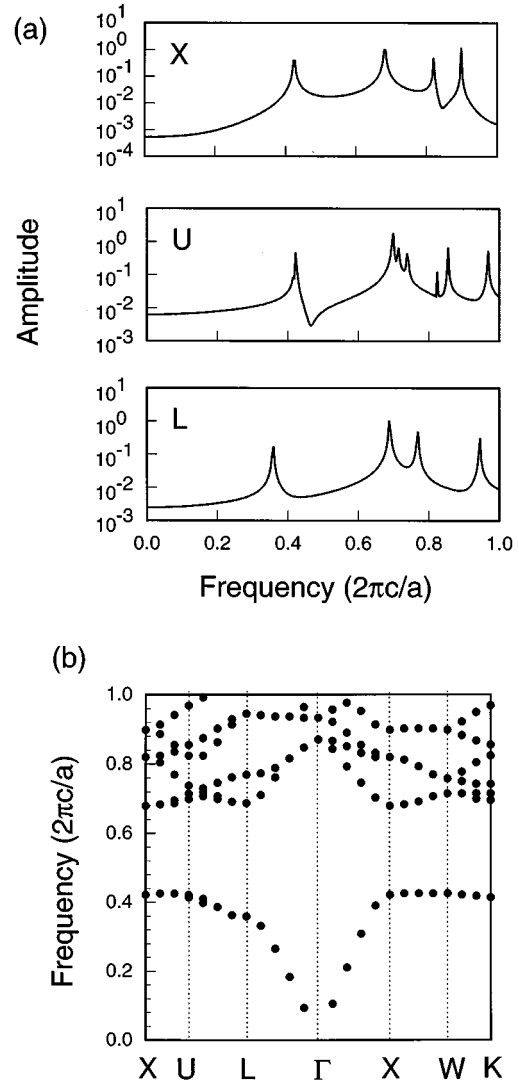


FIG. 5. (a) Spectral amplitude at several  $k$  points for the diamond structure of metallic spheres with  $r=0.21a$ . The spheres are embedded in Teflon ( $\epsilon=2.1$ ) (b) Band diagram for the same diamond structure. Each dot corresponds to a peak in the spectral amplitude at a specific wave vector.

mostly localized at the narrow region between the nearest-neighbor metal spheres.

The large frequency difference between the two modes can be explained using the variational theorem in electromagnetism, as described in Ref. 17:

$$\omega^2 = \frac{\int d\mathbf{r} \frac{1}{\epsilon} |\nabla \times \mathbf{H}|^2}{\int d\mathbf{r} \mathbf{H}^2}. \quad (2)$$

Equation (2) links the mode frequency with the spatial variation in the magnetic-field distribution. The band associated with the more extended magnetic field has a lower frequency, while the band with the more localized magnetic field has a higher frequency. The origin of the large gap is thus related to the sharp contrast in the spatial variation of the field distribution.

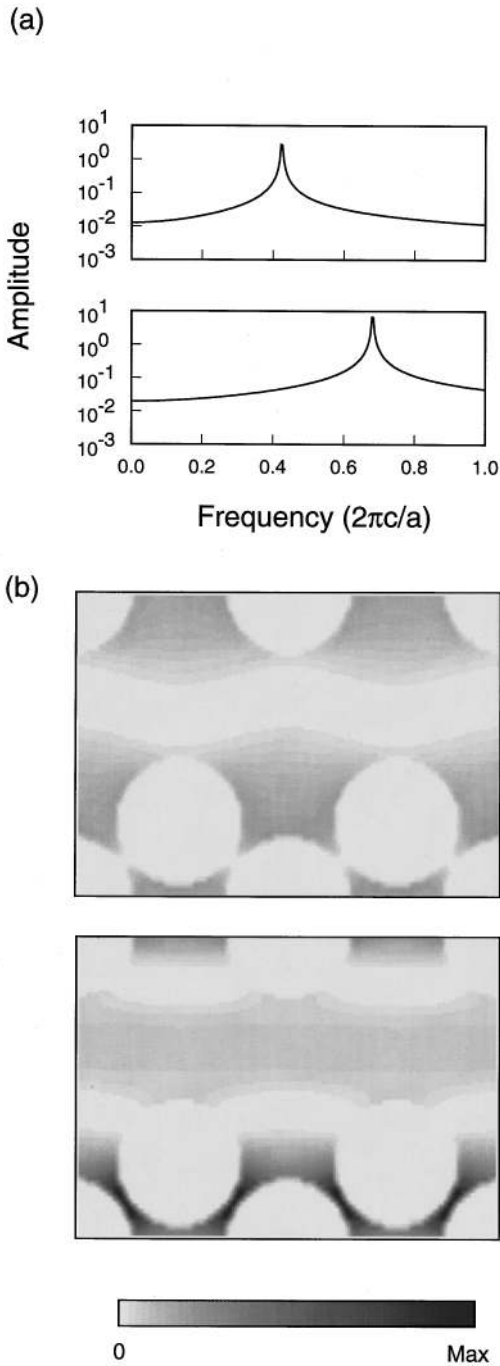


FIG. 6. Field distribution of two eigenstates in the diamond structures. Shown here are the two states at the edge of the gap at the  $X$  point. (a) Spectral amplitude. (b) Plot of the power density in the magnetic field on the  $(110)$  plane. In both cases, the top panels correspond to the state at the lower edge of the gap; the bottom panels correspond to the state at the upper edge of the gap.

### 3. Convergence

We study the convergence of our method by calculating the size of the gap at the  $X$  point using four different grid spacings ( $\delta s$ ):  $a/32$ ,  $a/64$ ,  $a/96$ , and  $a/128$ . The calculations are performed on four structures with different radii and the results are plotted in Fig. 7. For each structure the

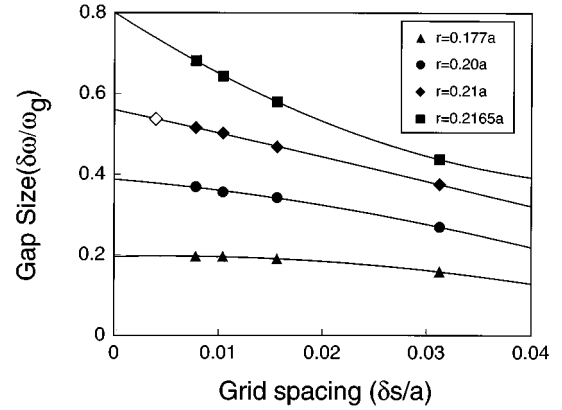


FIG. 7. Size of the gap at the  $X$  point as a function of grid spacing for four structures with  $r=0.177a$ ,  $0.20a$ ,  $0.21a$ , and  $0.2165a$ . For each structure a parabola is fitted and extrapolated to the limit where  $\delta s/a \rightarrow 0$ .

size of the gap increases with the grid density; however, the rate of convergence decreases as the spheres come closer to touching.

The convergence behavior is related to the field distribution of the eigenmodes, which has significant components in the area between the spheres. An accurate sampling of the fields in this region is important in order to obtain the precise frequency value and the gap size. This region, however, becomes smaller as the radius of the spheres increases, requiring a higher density of grid points for adequate sampling.

In using a finite-difference scheme to solve Maxwell's equations two types of errors occur. One type is caused by approximating the curls of the fields with a centered difference on the grid, while the other type comes from the staircase approximation for the metallic structure. In the first case, the error scales as  $(\delta s)^2$ , where  $\delta s$  is the grid spacing.<sup>9</sup> In the second case, the error originates from the uncertainty in representing the size of the air region between the nearest-neighbor spheres, which scales as  $\delta s$ . Consequently, the inaccuracy in the frequency or the gap size also scales as  $\delta s$ . The overall error in computing the size of the gap is a combination of both errors. We can therefore determine the size of the gap for each individual structure by fitting the results on a second-order polynomial with arguments  $\delta s$  and by extrapolating it to the limit where  $\delta s \rightarrow 0$ , as shown in Fig. 7.

### 4. Structural variations

We make a systematic examination of the photonic band structure as a function of the radius of the spheres. Calculations are performed using four different grid spacings and the results are plotted in Fig. 7. The extrapolated gap size for each structure is also shown. The gap increases rapidly as the spheres become larger and can be much greater than 60% when the radius exceeds  $0.21a$ .

In the case where the radius exceeds  $0.2165a$ , the spheres overlap and form a connected metallic network. As expected, when this occurs, the bands below the gap vanish leaving a gap from zero-frequency up to a cut-off frequency  $f_c$ . In the specific case where  $r=0.22a$ , the cut-off frequency is  $f_c = 0.45c/a$ .

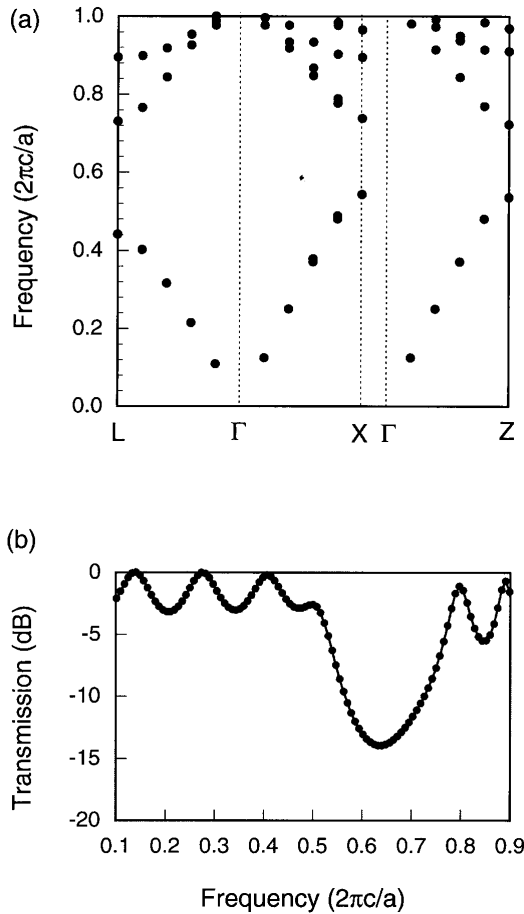


FIG. 8. Band diagram and transmission for a diamond structure of metallic spheres with radius  $r=0.21a$  embedded in Teflon ( $\epsilon=2.1$ ). The spheres are surrounded by air cylinders. (a) Band diagram for directions  $\Gamma$ -L,  $\Gamma$ -X, and  $\Gamma$ -Z. (b) Transmission through two cubic unit cells along the  $Z$  direction.

### 5. Fabrication

One possible approach for fabricating the diamond structure is to stack dielectric slabs, as proposed by Brown and McMahon for the fcc structure.<sup>2</sup> As an example, we assume Teflon slabs with  $\epsilon=2.1$ . A square lattice of cylindrical air holes with a lattice constant of  $0.70a$  can then be drilled on each side of the slab to house the metallic spheres. The holes on either side of the slab are shifted by  $0.35a$  with respect to each other. Each slab has a thickness of  $0.25a$ . The holes have a diameter of  $0.42a$  and a depth of  $0.21a$ . The holes on either side intersect each other. Each hole on one side of the slab is half filled with a metallic sphere of radius  $0.21a$ . The slabs are then stacked along the (100) direction in an  $ABCD$  staggered fashion so that the spheres extending beyond the surface of any given slab coincide with the holes at the bottom of the above slab. Such an arrangement of spheres generates a diamond lattice. The final step of the fabrication process would consist in covering the upper and the lower surfaces with a slab that is half as thick as the other ones, with an array of holes on only one side.

Photonic bands along some special directions are shown in Fig. 8(a). The degeneracy between the X and Z points is broken by the presence of the air cylinders. The wave vector

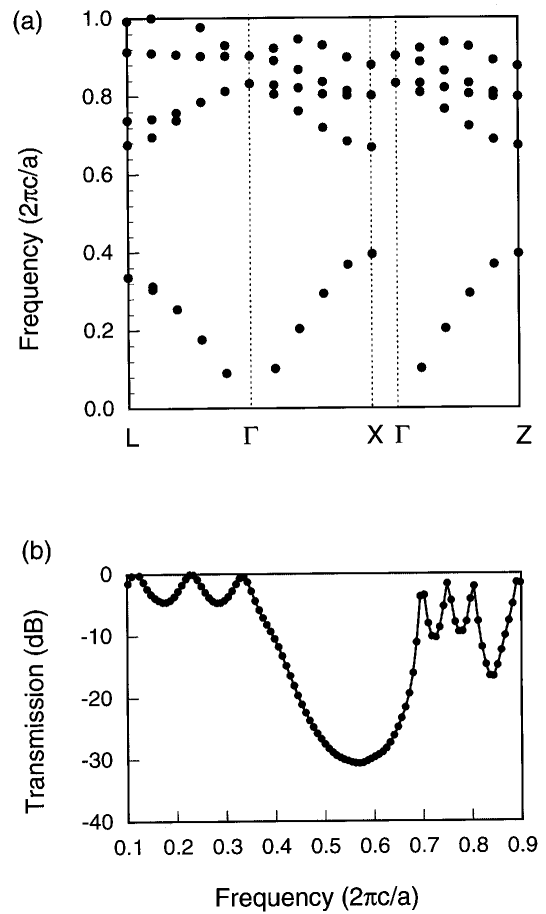


FIG. 9. Band diagram and transmission for a diamond structure of metallic spheres with radius  $r=0.21a$  embedded in Teflon ( $\epsilon=2.1$ ). The spheres are surrounded by cylinders filled with resin ( $\epsilon=2.5$ ). (a) Band diagram for directions  $\Gamma$ -L,  $\Gamma$ -X, and  $\Gamma$ -Z. (b) Transmission through two cubic unit cells along the  $Z$  direction.

at the Z point is normal to the slabs. The gap at Z extends from frequency  $f=0.54c/a$  to  $0.72c/a$ , which yields a gap of 28.5%. The transmission normal to the slab through two cubic unit cells is shown in Fig. 8(b). The maximum rejection is 14 dB, or 7 dB per lattice constant, occurring at a frequency of  $0.64c/a$ , which is close to the midgap frequency.

In order to prevent the nearest-neighbor spheres from touching, Brown has suggested filling the air voids in the cylinders with resin.<sup>18</sup> Since resin has a higher dielectric constant ( $\epsilon=2.5$ ), the frequencies decrease in both the upper and lower bands. The lower band, however, is affected more strongly since the associated electric fields are concentrated between the spheres.<sup>19</sup> As a result, the gap widens significantly to a size of 53%, extending from frequency  $f=0.39c/a$  to  $0.67c/a$ , as shown in Fig. 9(a). The maximum rejection also increases to 31 dB, or 15.5 dB per lattice constant, with the same sample containing two cubic unit cells [Fig. 9(b)].

### IV. SUMMARY

We have successfully applied a FDTD method to obtain both the band-structure and the transmission properties of metallodielectric photonic crystals. Excellent agreement is

obtained between our theory and available experimental data on a fcc structure. We further predict that a diamond lattice of metallic spheres will give rise to an omnidirectional photonic band gap, the size of which can be larger than the size of the gap in conventional all-dielectric photonic crystals. We propose a possible fabrication scheme for these structures and compute the transmission spectra that could be used for a direct comparison with experiments.

*Note added in proof.* We computed the size of the gap in the diamond structure with a grid spacing  $\delta s$  of  $a/256$  for  $r=0.21a$ . The extra point was added to Fig. 7 after the ex-

trapolation. The point lies directly on top of the curve, which validates our extrapolation scheme.

#### ACKNOWLEDGMENTS

The authors acknowledge useful discussions with E. R. Brown, J. C. Chen, K. Cho, and T. A. Arias and computational support from D. S. Abrams. The work is supported in part by Army Research Office Grant No. DAAH04-93-G-0262 and the MRSEC Program of the NSF under Grant No. DMR-9400334.

- 
- <sup>1</sup>D. R. Smith, S. Schultz, N. Kroll, M. Sigalas, K. M. Ho, and C. M. Soukoulis, *Appl. Phys. Lett.* **65**, 645 (1994).  
<sup>2</sup>E. R. Brown and O. B. McMahon, *Appl. Phys. Lett.* **67**, 2138 (1995).  
<sup>3</sup>D. F. Sievenpiper, M. E. Sickmiller, and E. Yablonovitch, *Phys. Rev. Lett.* **76**, 2480 (1996).  
<sup>4</sup>A. R. McGurn and A. A. Maradudin, *Phys. Rev. B* **48**, 17 576 (1993).  
<sup>5</sup>J. B. Pendry, *J. Mod. Opt.* **41**, 109 (1994).  
<sup>6</sup>V. Kuzmiak, A. A. Maradudin, and F. Pinceman, *Phys. Rev. B* **50**, 16 835 (1994).  
<sup>7</sup>N. A. Nicorovici, R. C. McPhedran, and L. C. Botten, *Phys. Rev. Lett.* **75**, 1507 (1995); *Phys. Rev. E* **52**, 1135 (1995).  
<sup>8</sup>M. M. Sigalas, C. T. Chan, K. M. Ho, and C. M. Soukoulis, *Phys. Rev. B* **52**, 17 744 (1995).  
<sup>9</sup>See, for example, E. K. Miller, *J. Electromagn. Waves Appl.* **8**, 1125 (1994); K. S. Kunz and R. J. Luebbers, *The Finite Difference Time Domain Method for Electromagnetics* (CRC, Boca Raton, FL, 1993).  
<sup>10</sup>K. S. Yee, *IEEE Trans. Antennas Propagat.* **AP-14**, 302 (1966).  
<sup>11</sup>A. C. Cangellaris and D. B. Wright, *IEEE Trans. Antennas Propagat.* **AP-39**, 1518 (1991).  
<sup>12</sup>G. Mur, *IEEE Trans. Electromagn. Compat.* **EMC-23**, 377 (1981).  
<sup>13</sup>T. A. Arias, M. C. Payne, and J. D. Joannopoulos, *Phys. Rev. B* **45**, 1538 (1992).  
<sup>14</sup>C. T. Chan, Q. L. Yu, and K. M. Ho, *Phys. Rev. B* **51**, 16 635 (1995).  
<sup>15</sup>K. M. Ho, C. T. Chan, and C. M. Soukoulis, *Phys. Rev. Lett.* **65**, 3152 (1990).  
<sup>16</sup>R. D. Meade, A. M. Rappe, K. D. Brommer, and J. D. Joannopoulos, *J. Opt. Soc. Am. B* **10**, 328 (1993).  
<sup>17</sup>J. D. Joannopoulos, R. D. Meade, and J. N. Winn, *Photonic Crystals, Molding the Flow of Light* (Princeton University Press, Princeton, 1995).  
<sup>18</sup>E. R. Brown (private communication).  
<sup>19</sup>The *magnetic*-field distribution is shown in Fig. 6(b). The *magnetic* field associated with the lower band at the Z point is extended throughout the open region. In contrast, the *electric* field corresponding to the same band is concentrated in the region between the spheres. The electric field associated with the upper band is distributed throughout the open region.